

Distortion of DNA Origami on Graphene Imaged with Advanced TEM Techniques

Yoones Kabiri, Adithya N. Ananth, Jaco van der Torre, Allard Katan, Jin-Yong Hong, Sairam Malladi, Jing Kong, Henny Zandbergen,* and Cees Dekker*

While graphene may appear to be the ultimate support membrane for transmission electron microscopy (TEM) imaging of DNA nanostructures, very little is known if it poses an advantage over conventional carbon supports in terms of resolution and contrast. Microscopic investigations are carried out on DNA origami nanoplates that are supported onto freestanding graphene, using advanced TEM techniques, including a new dark-field technique that is recently developed in our lab. TEM images of stained and unstained DNA origami are presented with high contrast on both graphene and amorphous carbon membranes. On graphene, the images of the origami plates show severe unwanted distortions, where the rectangular shape of the nanoplates is significantly distorted. From a number of comparative control experiments, it is demonstrated that neither staining agents, nor screening ions, nor the level of electron-beam irradiation cause this distortion. Instead, it is suggested that origami nanoplates are distorted due to hydrophobic interaction of the DNA bases with graphene upon adsorption of the DNA origami nanoplates.

1. Introduction

Graphene features tantalizing properties suitable for a wide range of applications, from next-generation nanoelectronics and biosensing to transmission electron microscopy (TEM) imaging of biomolecules.^[1–3] Graphene gained an interest in the TEM community as a support substrate because it can be as thin as one carbon atom, which provides the lowest cross-section for elastic and inelastic scattering.^[4] Moreover,

graphene mitigates electron-beam-associated damage.^[4,5] As a result, high-resolution, high-contrast images can be obtained for weak-phase objects that are supported onto or sandwiched between graphene layers.^[4,6]

Can graphene also facilitate the imaging of (unstained) nucleic acids with TEM? Here, we address this question by utilizing DNA origami test structures. Such DNA origami, DNA that is folded into well-defined shapes, is an emerging workhorse for synthetic biology and programmable materials due to its accessible and compelling self-assembly principle.^[7–10] 2D DNA origami is an excellent microscopy test object as it features the same scattering properties as double-stranded DNA, while it comes with a bigger and defined size, which helps the observation and investigation.

To the best of our knowledge, no high-resolution TEM (HRTEM) imaging of origami has been reported without staining or class averaging, since various challenges arise for HRTEM imaging of biological specimens in general and DNA macromolecular assemblies in particular, such as sample preparation, beam damage, inherently low contrast of nucleic acids, and substrate signal contributions.^[11] Some attempts of direct imaging of unstained DNA have

Y. Kabiri, A. N. Ananth, J. van der Torre, Dr. A. Katan,
Dr. S. Malladi, Prof. H. Zandbergen, Prof. C. Dekker
Kavli Institute of Nanoscience Delft
Delft University of Technology
Delft 2629HZ, The Netherlands
E-mail: h.w.zandbergen@tudelft.nl; c.dekker@tudelft.nl



Dr. J.-Y. Hong, Prof. J. Kong
Department of Electrical Engineering and Computer Science
Massachusetts Institute of Technology
Cambridge, MA 02139, USA

DOI: 10.1002/sml.201700876

already been reported.^[12–14] However, even when deposited onto an atomically thin layer of graphene, unstained DNA structures are barely distinguishable in normal TEM mode due to their low scattering elements.^[4,15] This necessitates further developments in electron optics for their visualization. The common practice in life science TEM is to enhance the contrast at the expense of losing resolution by strongly defocusing the objective lens (by 1–10 μm), i.e., transforming part of the phase information into amplitude. Such a methodology, however, is not suitable for high-resolution imaging due to information delocalization.^[16]

In order to boost the in-focus contrast for nucleic acids, we employ two complementary TEM techniques, viz., scanning transmission electron microscopy (STEM) and a special type of dark-field (DF) microscopy. STEM and DF allowed us to shed light on the conformational polymorphism of DNA origami on graphene without the need for any staining compound and class averaging. So far, only stained or class-averaged images of origami on carbon membranes were reported in literature. Since our imaging techniques provide good contrast as well as sufficient resolution for visualization, we could notice an unexpected behavior of the origami plates onto graphene, namely, that crumpled and deformed rectangles were obtained instead of fully flat and rectangular structures that are normally observed onto amorphous carbon supports. A range of complementary characterization techniques, provided in this paper, examine various parameters on the imaging of the origami plates, such as staining or screening ions, the level of electron-beam irradiation, and surface interaction of the origami plates with graphene.

2. Results and Discussions

We first characterized the DNA origami plates using liquid-cell atomic force microscopy (AFM). **Figure 1b** depicts a typical AFM image of the origami on a mica surface in liquid. It is seen that nanoplates are well dispersed on the mica surface with a suitable density for imaging. AFM was the fastest way to control the folding and purification success and was the basic control that we did prior to TEM sample preparations. Liquid-cell AFM was essential, as we found problems in AFM imaging in dry condition, such as curvature at the bottom of the plates, side arms sticking to one another, and concealment of the smaller cavity (observed for more than 95% of the plates tested for various Mg^{2+} ionic strength, see Figure S1 in the Supporting Information). In liquid, on the other hand, the AFM images (Figure 1b) conform to the computer design. A slight distortion in aspect ratio is noticed, similar to

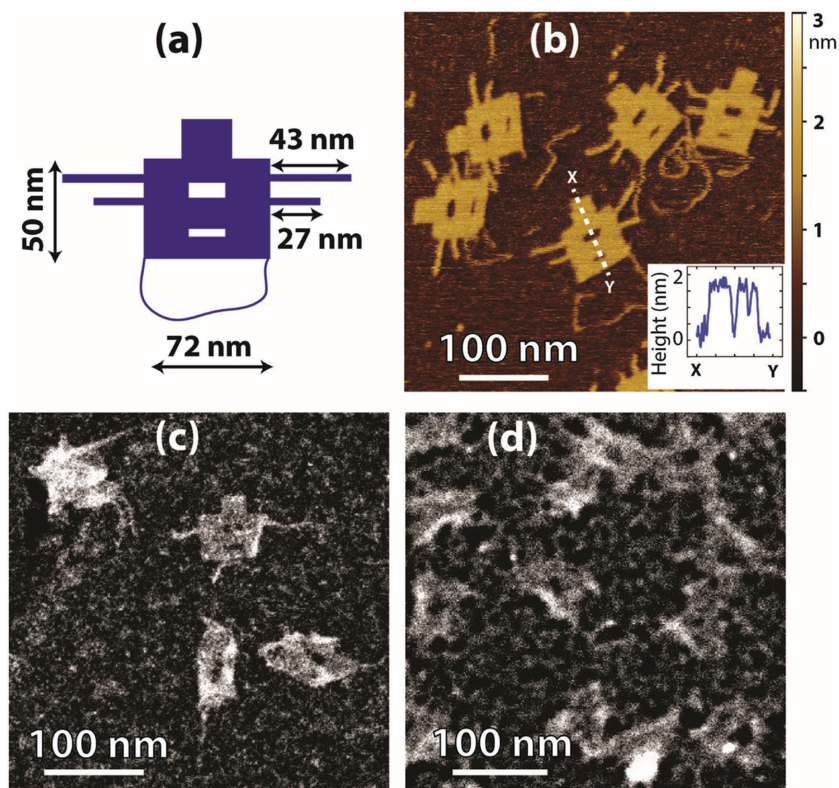


Figure 1. a) Design schematic of the symmetric DNA origami nanoplate. b) Liquid-cell AFM image of DNA origami on mica. c) Uranyl acetate stained DNA origami plates on suspended graphene imaged with STEM. d) Same, but without any staining.

earlier reports by Rothmund in his original paper,^[9] where he observed origami rectangles changing into a slightly hour-glass-shaped structure due to imaging artifacts. The dsDNA loop at the bottom of the plate was quite floppy in liquid and we added 1×10^{-3} M NiCl_2 in the buffer to immobilize the loop onto the surface.

After characterization of the origami structures with AFM, we turned to TEM for imaging them on freestanding graphene, which is the main focus of this paper. We started by imaging uranyl-stained origami on graphene by STEM, which provides the best contrast. We mostly found white “blobs,” which were hardly distinguishable as DNA origami plate. Extensive imaging was carried out to make sure that our observation was indeed valid for all TEM samples. Figure 1c shows the best image that we could acquire in our dataset. The most striking observation is that the majority of the investigated nanoplates seem to show very crumpled conformations. To our surprise, DNA origami plates thus appear to be severely distorted upon adsorption onto graphene. Several attempts were made to improve the images such as graphene cleaning, changing Mg^{2+} concentration in a range of 15×10^{-3} to 60×10^{-3} M, and removing ethylenediaminetetraacetic acid (EDTA) from the buffer (Figure S2, Supporting Information). All these efforts failed to tackle the distortion problem. In the remaining part of the paper, we will examine what underlies this distortion.

We found out that distortion occurs regardless of the staining. DNA nanostructures are weak-phase objects for

TEM, and staining agents that contain high-scattering elements such as heavy metals, are commonly utilized to increase the contrast. As a consequence of the binding of staining agents, artifacts can occur, e.g., double helix unwinding, DNA lengthening, kink formation, and intrastrand cross-linking.^[17] In view of the distortion shown in Figure 1c, we wondered whether the staining could be the reason. To examine this, we acquired images of unstained origami on graphene. It should be noted that this is not possible with conventional TEM, even on graphene.^[4] A better approach is using STEM, where a high-angle annular dark-field (HAADF) detector is utilized to collect the Rutherford-scattered electrons. The STEM contrast scales with Z^2 (or more precisely, the exponent of Z is reported to be between 1.6 and 1.8 instead of the classical value of 2),^[18] which theoretically makes it possible to distinguish DNA (rich in phosphorous with $Z = 15$) on graphene ($Z = 6$). One example of a STEM image of unstained origami on graphene is presented in Figure 1d. Incidentally, we mention that it is noteworthy to present such an image since TEM images of single-layer unstained DNA origami are rare. Similar to our observations for the stained origami, we present the best image for the unstained one. It can be seen that the majority of the nanoplates depict the same severe structural deformation despite the absence of uranyl acetate stain. Again, various attempts such as changing Mg^{2+} concentration, removing EDTA from the buffer, or testing on different batch of graphene did not improve the images in terms of seeing DNA origami structures with all the design components. The comparison of Figure 1c,d thus shows that uranyl staining does not cause the origami distortion. Later in the paper, we show that our TEM techniques are indeed able to visualize even a single DNA helix. However, the severe distortion of DNA on graphene greatly smears the contrast that can be obtained.

The distortion of the DNA origami is also not caused by the electron beam, as could be conceived for a highly focused STEM probe. The good contrast in Figure 1c,d is due to high signal-to-noise ratio (SNR) of the focused STEM beam, but the strongly focused beam can cause severe structural damage.^[19–21] In general, the applicability of STEM to image polymeric materials, including nucleic acid macromolecules, should be cautiously examined. We thus speculated whether the distortion might be due to STEM-induced damage, leading to crumpling of nanoplates. Therefore, we also probed the nanoplates with a broad parallel beam, where we circumvented the low-SNR problem in wide-field TEM using our newly developed DF technique (see the Experimental

Section for more details on the DF technique in detail).^[22] For a fair comparison, we acquired images on the exact same area, first exposing the region of interest with wide-field (DF image in **Figure 2**) and subsequently with a focused beam (STEM image in **Figure 2**). No difference was seen between sequential images in panels (b) and (c), not only for this particular region but also for the entire area of the TEM grids. Thus, these experiments exclude STEM-associated damage as the origin of the observed nanoplate crumpling.

Before we move on, we address several points in **Figure 2** that are worthy of consideration: 1) In contrast to TEM imaging on amorphous carbon substrates, electron-induced contamination^[23] is not observed on the graphene substrates such as in **Figure 2a**, even after several exposures on the boxed area. This hints on the damage-mitigation property of graphene reported earlier by Algara-Siller et al.,^[24] which was attributed to the high thermal and electrical conductivity of graphene. The properties of graphene are also advantageous in terms of sample drift and charging,

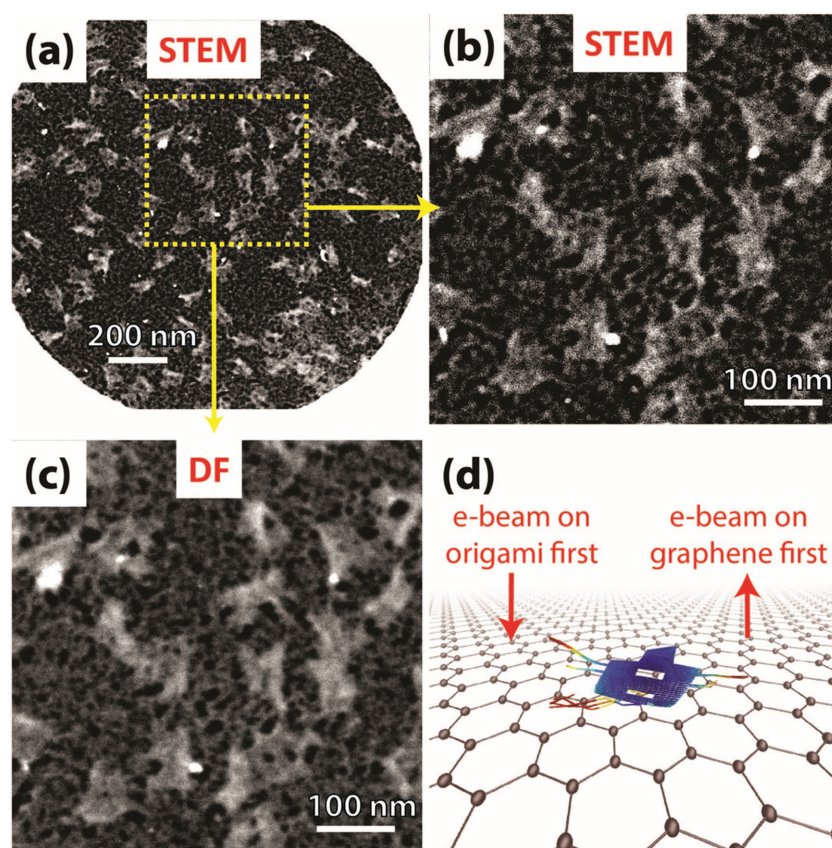


Figure 2. Comparison of STEM and DF to examine the effect of beam exposure on DNA origami distortion. a) STEM overview image of the investigated area of unstained DNA origami on graphene. b) Close-up of the boxed area in (a) imaged with STEM. c) Same for DF. Note that the sequence of events during imaging was from (c) to (a) in order to expose the area first with DF and only then with STEM. The DNA origami appears to be the same in panels (c) and (b), which shows that the intense STEM beam does not cause the distortion. Focus setting of the microscope was carried out in the neighboring area to avoid beam damage on the region of interest. The electron dose for the DF image in (c) corresponds to $25 \text{ e } \text{Å}^{-2}$. Similar distorted DNA plates were seen when imaged with lower electron doses. d) Artistic impression of origami on graphene (not to scale). Two different orientations were investigated: one where the electron beam first hits the origami and then graphene (left arrow), or the other way round (right arrow). We did not observe any difference in terms of damage response.

allowing improved HRTEM imaging. 2) By comparing Figure 2b,c, it is seen that the contrast enhancement obtained in the DF is comparable to that of STEM. Considering that most TEM labs around the world lack access to deflecting-coil STEM, using a “Mercedes star” in the objective aperture cassette suggests a cheap and easy alternative for contrast enhancement. Since the central beam is absent, the intensity reaching the camera is too low in the DF technique, where the noise becomes an important factor (the central beam contributes to more than 99% of the intensity in a normal bright-field image of graphene).^[22] Therefore, contrast can be further improved by removing the noise in the CCD cameras. Obviously, using the recent direct electron detection technology is advantageous in this regard.^[25] 3) We also examined whether the distortion was an effect of sample orientation relative to the electron beam, i.e., if the electrons first hit the sample and then the graphene, or vice versa (note the two arrow directions in Figure 2d). Several studies reported such an orientation-dependent damage response in beam-sensitive materials, especially for materials containing light elements.^[5,19,24] For our origami sample, sputtering of light atoms from the DNA structure might be a reason behind the crumpling of nanoplates. However, we did not observe any dependence on sample orientation relative to the electron beam, as in both cases, distorted plates were seen. 4) The background of the DNA origami images on graphene indicates the presence of contaminants. Likely, these are origami buffer constituents,^[4] hydrocarbon contaminations,^[4,26] or contaminants that result from graphene transfer.

Finally, we show that the distortion is dependent on which substrate the origami plates are deposited on. So far, we ruled out staining and imaging artifacts as the origin of origami damage on graphene. One other parameter to consider is the interaction of origami with graphene. It has been suggested that this interaction is mediated through π - π stacking of the aromatic purine and pyrimidine DNA bases with the delocalized π bonds of graphene.^[27] To test this, we examined origami behavior on amorphous carbon film as an alternative substrate, where such π - π interactions will be absent. **Figure 3** shows that the origami is well flattened on the amorphous carbon, depicting all the details encoded in the computer design (cf. Figure 1a). Note that remarkably we obtain good contrast of a 2-nm-thin uranyl-stained DNA on a 15-nm-thick carbon support (thickness of carbon measured by electron energy loss spectroscopy (EELS)). The nice images in Figure 3 incidentally prove that origami is stable under vacuum condition of the microscope (10^{-7} mbar) as

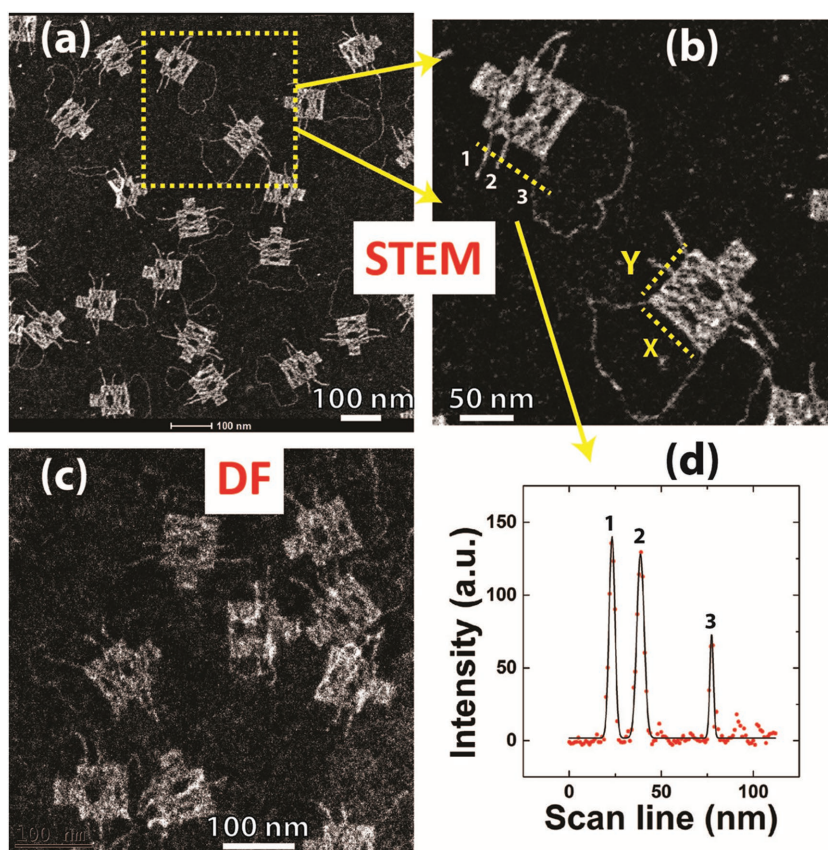


Figure 3. Distortion of the DNA origami is found to be substrate dependent. On amorphous carbon, origami is well spread and all details of the nanoplates become visible. a) STEM image of uranyl-stained origami on 15-nm amorphous carbon (thickness measured by EELS). b) Close-up of dashed area in (a). All structural features in the nanoplate design (cf. Figure 1a) are resolved. X and Y correspond to 71 and 65 nm, respectively. c) DF image on the same carbon membrane but from a different area. DF can also visualize the structures, however, with a lower SNR. d) Line profile of the detector signal passing through the DNA bundles and single dsDNA loop indicated by the dashed line in panel (b). The peaks depict an excellent contrast with high SNR. We find full widths at half maxima of 3.4, 4.3, and 2.1 nm corresponding to peaks 1–3. These values conform to the widths of 2-helix DNA bundles (4 nm wide) and single dsDNA (2 nm wide) (cf. Figure 1a).

well as during image acquisitions (both with STEM and DF at 300 kV at room temperature).

We find that DNA origami is also distorted when deposited onto highly oriented pyrolytic graphite (HOPG), which has a surface very similar to that of graphene. Although this may seem trivial, there is no consensus on whether and how DNA origami interacts with the HOPG surface.^[27–31] The different reported results may be due to different experimental conditions including buffer, pH, salt concentrations, or biased sampling of the imaging area. Lacking a proper comprehensive study, we carried out our own AFM experiments. **Figure 4a** shows the DNA origami structures on HOPG that are so heavily disconfigured that they are barely identifiable as rectangles. Control experiments (Figure S3, Supporting Information) proved that the observed structures on HOPG are indeed DNA and not hydrophobic contaminants.

The interaction of the origami plates and graphene can be prevented by surface functionalization. We passivated HOPG and graphene surfaces with polylysine (PLL) and with 1-pyrenecarboxylic acid (1PCA)^[32] respectively, and performed

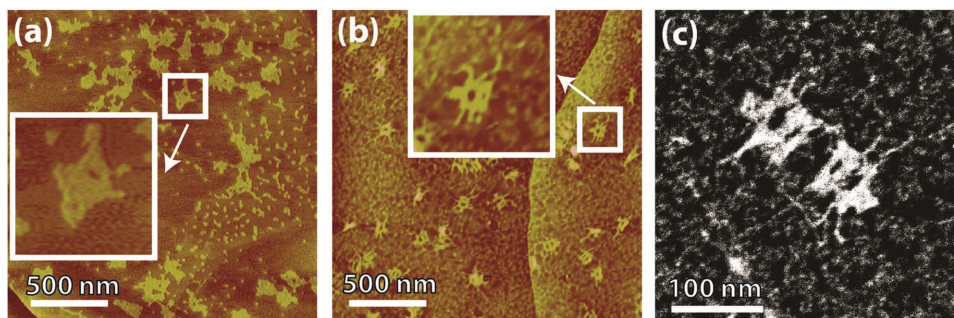


Figure 4. Graphene functionalization prevents π - π stacking with the hydrophobic DNA bases. a) AFM image of origami on a HOPG surface. b) Origami on a PLL-coated HOPG. Insets are enlargements of the plates marked inside the boxes. c) STEM image of a stained origami on 1PCA-functionalized graphene, showing less distorted plates compared to bare graphene.

AFM and TEM analysis. Figure 4b shows a typical AFM image of the origami plates onto a PLL-coated HOPG surface. By comparing the images of the DNA origami onto bare HOPG and PLL-coated HOPG surfaces (panel a and b in Figure 4), it is clear that PLL coating on HOPG prevents adverse interactions between the HOPG and the origami. Although the origami plates in Figure 4b are a bit distorted compared to Figure 1b (onto mica), the integrity of the structure is well maintained. We see a similar trend in TEM images of origami plates deposited onto bare and 1PCA-functionalized graphene. Figure 4c illustrates a typical STEM image that we acquired onto 1PCA-functionalized graphene. While the images of the origami plates on bare graphene show very distorted conformation (cf. Figures 1 and 2), we see much less distortion in Figure 4c, where for example, the cavities inside the plates become visible. From both AFM and TEM experiments on functionalized HOPG and graphene surfaces, we thus can conclude that the interaction between the origami plates and graphene plays a crucial role in the observed distortion.

To quantify the distortion, we define a parameter D as the surface area of the observed origami image divided by its theoretical surface area. For example, a value of $D = 0.5$ represents a distorted nanoplate that has a surface area equal to only half the expected size. For calculation of the theoretical size according to the design sketch in Figure 1a, we need to consider a subtle point, namely that the origami structures are extended along the y -axis. Multiple works have previously demonstrated that 2D origami plates cannot strictly be modeled as a series of closely-packed parallel double helices.^[9,33] In typical buffer conditions, electrostatic forces between the negatively charged strands cause interhelical gaps (see **Figure 5a**). Hence, we calculate the size of the origami plate as follows. With n as the number of base pairs along the x -axis, the width X of the origami plate can be estimated as $X = n \times 0.34$ nm. However, the height Y of the origami does not simply follow a $2 \times h$ equation (with h as the number of double-stranded helices along the y -axis, and 2 nm as the width for B-form DNA; note that $h = 25$ in our design). Instead, a modified expression $Y = 2h + g(h - 1)$ should be used, where g is the size of the interhelical gap caused by the electrostatic repulsion between the strands.^[33] The gap size g may vary depending on ionic strength or the design parameters. Since there is no computational method available for

size estimation, liquid-cell AFM remains the easiest experimental way to measure the true dimensions of the origami. Figure 5b summarizes our liquid-cell AFM measurements of the origami size. In accord with the TEM data as well as with theoretical calculations, we find a consistent value for the nanoplate width of $X = 72.8 \pm 2.2$ nm (mean \pm standard deviation), whereas the height of the structure is $Y = 67.2 \pm 4.4$ nm. From these values, we extracted the surface area of the nanoplate. Based on the obtained true size from the AFM experiments, we now return to the TEM image analysis. We processed the distortion of about 50 randomly selected origami plates in the TEM images taken from each substrate (graphene, 1PCA-functionalized graphene, and amorphous carbon), and report the result in Figure 5c. In accord with the shown TEM data (Figures 1, 2, 3), the statistical analysis in Figure 5c shows that most nanoplates are indeed severely crumpled to almost one-third of their size, $D = 0.37 \pm 0.08$ (mean \pm standard deviation), whereas they are much less distorted on carbon substrate, $D = 0.85 \pm 0.10$. For the 1PCA-functionalized graphene, D equals 0.58 ± 0.14 , which falls in between the values for the graphene and carbon substrates. The statistical analysis thus shows that the substrates made from the same carbon element but with different hydrophobic surface properties result in significantly different D values.

3. Conclusion

With high-resolution STEM and DF techniques, we were able to image for the first time both stained and unstained DNA origami nanoplates on graphene and amorphous carbon membranes with good contrast. We observed that origami nanoplates exhibited a structural distortion when deposited onto graphene. Through a range of complementary control experiments, we conclude that the distortion can be attributed to the interaction of DNA with graphene, likely through π - π bonds. After quantification of the distortion onto different substrates, we found significant different mean values of the relative area of the origami plates, which quantitatively supports our observation in the presented TEM images. We conclude that while graphene provides the ultimate thin and strong sample support for materials science or some biological samples,^[3] its applicability to DNA nanostructures is hindered by π - π interactions.

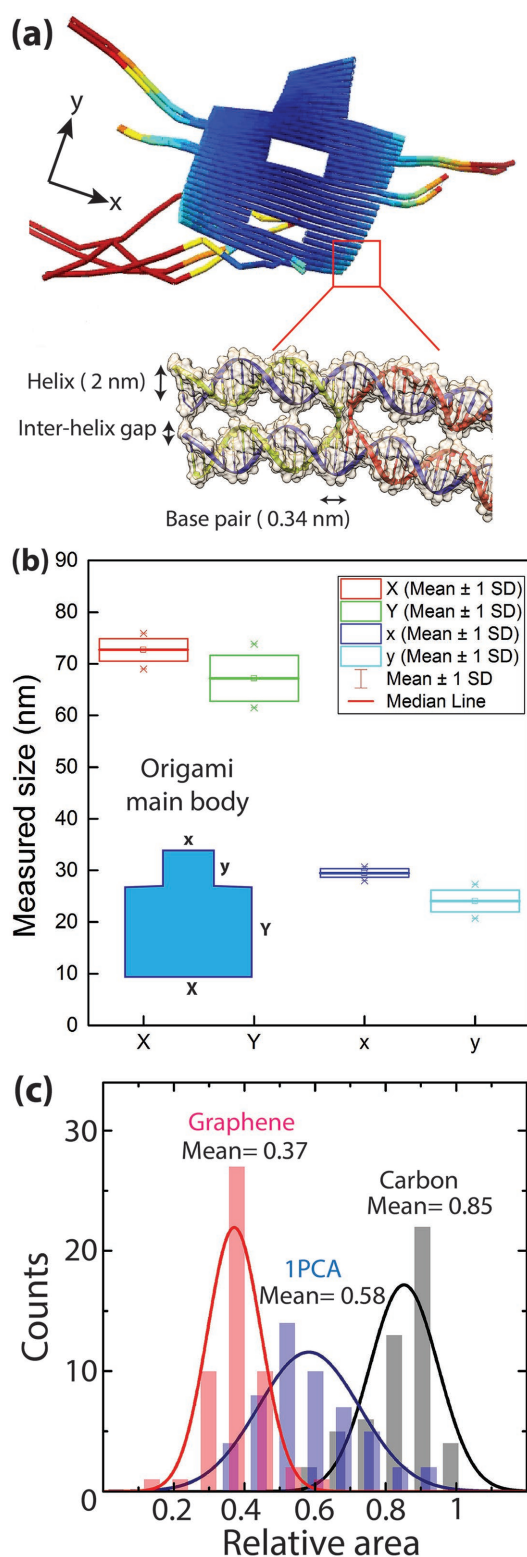


Figure 5. Quantification of the distortion of DNA origami on graphene-like substrates. a) Interhelical gaps along the y-axis of the nanoplate caused by electrostatic repulsions between the strands (the origami snapshot is exported from the caDNA package). b) Liquid-cell AFM measurements of the nanoplate dimensions. c) Statistical analysis of the relative area of origami plates extracted from TEM images onto different substrates (graphene, 1PCA-functionalized graphene, and amorphous carbon). We find significant different mean values for the relative area on different substrates.

4. Experimental Section

Graphene Growth, Transfer, and Quality Characterization: Single-layer CVD-grown graphene was used to have large available areas for TEM investigations. Details of CVD growth and Raman spectroscopy for the growth characterization are given in Figure S4 in the Supporting Information. In order to avoid polymer residues, graphene was transferred to TEM grids (Quantifoil, gold coated, 200 mesh) using a dry-transfer method (Figure S5, Supporting Information).^[34] Grids were examined by a number of TEM techniques to ensure layer thickness and cleanliness (Figure S6, Supporting Information). Note that no hydrophilic treatment such as glow discharging was performed on the grids, as graphene is very susceptible to even gentle plasma treatment.

Origami Design, Assembly, and Purification: As a test object for TEM imaging, we designed a 2D DNA origami structure (Figure 1a) using caDNA package.^[10] We aimed to create a symmetric structure that can be well recognized in imaging. A 50×72 nm rectangular plate was designed with a number of different elements such as cavities in the middle (4 and 8 nm wide, 19 nm long), DNA bundles on the side arms (4 nm wide, 27 and 43 nm long), and a floppy dsDNA loop at the bottom (2 nm wide). For a detailed scheme of the design, see Figure S7 in the Supporting Information. Note that the structure is a 2D design, which means that it is only one dsDNA thick (2 nm), which is desired as we aim for TEM visualization of single dsDNA structures. The structure is a suitable microscopy test object in order to check if different TEM techniques (STEM, DF) can provide enough resolution to visualize DNA at various length scales in the design.

To fold the origami plate, a 7560 base-long scaffold (M13mp18 phage-derived genomic DNA), and staple oligonucleotide strands were purchased from Tilibit, Munich, Germany. Folding reactions consisted of folding buffer (5×10^{-3} M Tris-base, 1×10^{-3} M EDTA, 5×10^{-3} M NaCl, and 12.5×10^{-3} M $MgCl_2$ at pH 8), 20×10^{-9} M scaffold strand supplied with $10\times$ excess oligo staples (200×10^{-9} M). A thermocycler was used to fold the structure by heating first to 65 °C and then ramping the temperature from 60 to 40 °C at a cooling rate of 1 °C h⁻¹ and subsequently keeping the nanostructures at 12 °C. After folding, origami plates were purified from excess staple oligonucleotides using Amicon cutoff filters (100 kDa, Milipore). Prior to centrifugation, the filter membranes were preconditioned with the working buffer (10×10^{-3} M Tris-base, 1×10^{-3} M EDTA, pH 8, 15×10^{-3} M $MgCl_2$, 5×10^{-3} M NaCl at pH 8). Four cycles of purification (2200 rcf, 4 °C) removed most oligos (Figure S8, Supporting Information). The remaining solution in the dead volume of the filter was collected and diluted to a final origami concentration of 5×10^{-9} M for TEM sample preparation. Oligomer sequences, finite-element simulations, and gel electrophoresis results (for both purified and unpurified plates) are given in the Supporting Information.

TEM Sample Preparations: 5 μ L of origami nanoplates (oligo purified, 5×10^{-9} M) was drop casted onto graphene-coated TEM grids and incubated for 2 min. Subsequently, the samples were washed with Milli-Q (MQ) water to remove unadhered origamis, and excess MQ from the washing step was blotted away. For the stained samples, immediately after washing away the excess origamis, staining agent was applied (2% uranyl acetate in MQ, filtered through a 0.2- μ m PTFE membrane), incubated for 1 min, and washed with MQ. We also prepared origami samples onto

amorphous carbon grids (nominal 4-nm carbon onto 6-nm formvar-coated TEM grids, Electron Microscopy Science, USA), followed by the same protocol as mentioned for origami on graphene, but after rendering the carbon hydrophilic with nitrogen plasma.

TEM Imaging: All STEM/DF images were taken with an FEI Titan microscope equipped with post-specimen aberration corrector under 300 kV operating voltage. The third-order spherical-aberration coefficient (C_3) was tuned to zero in the image corrector for all S/TEM alignments to minimize the delocalization. Utilization of a HAADF detector at a camera length of 28.3 cm resulted in mass-thickness dominated contrast. No class averaging was done and all images are single acquisitions at near zero focus.

In the conventional dark-field technique, certain spatial frequencies in the back-focal plane are collected by the objective aperture to form the image. In our DF method, in contrast, all scattered frequencies are let through, except the noise-bearing central beam.^[22] To realize this, we fabricated a “Mercedes star”-shaped aperture on a 5- μm -thick platinum foil and ion-milled the Mercedes star using an FEI Helios microscope. Special care was taken to fabricate an as-smooth-as-possible aperture to avoid beam charging and image drift. Detailed geometry and dimensions of the delicate DF aperture are provided in Figure S9 in the Supporting Information, as well as an electron optical comparison with STEM (Figure S10, Supporting Information). The DF aperture achieves a 1 Å information cutoff (Figure S10c, Supporting Information). We have previously shown that an information cutoff beyond 1 Å would have a minimal effect on the contrast of weak-phase objects such as DNA origami supported onto graphene, whereas removal of the central beam has a major effect due to elimination of the Poisson noise.^[22] Therefore, 1 Å information cutoff seems satisfactory for the DF aperture. Collection of all scattered electrons while omitting the central beam results in a dramatic contrast enhancement, as shown on a graphene test sample in Figure S11 in the Supporting Information. In contrast to conventional bright-field imaging, the interference of diffracted beams enhances the contrast in our DF technique (nonlinear imaging).^[22] Note that for complete blockade of the central beam, parallel illumination is a prerequisite. Hence, the C3 lens in the condenser system of the Titan microscope should be well tuned. We did DF image simulations to find the optimum focus for imaging. Based on our simulations (Figures S12 and S13, Supporting Information), the best contrast is achieved at near zero focus with a C_3 -corrected microscope. Finally, it should be mentioned that the temperature rise during STEM/DF imaging is negligible (only 1–2 K)^[23] and will not cause any structural melting under the electron beam (as double-helix unwinding only occurs above 50 °C).

AFM Imaging: AFM investigations were carried out on freshly cleaved surfaces of mica and HOPG under dry condition unless indicated otherwise. Note that 4 μL of origami sample (5×10^{-9} M) was drop casted onto 3 mm wide mica or HOPG disks, incubated for 1 min, washed three times with MQ, and finally blown dry with nitrogen gas. Image acquisition was carried out in tapping mode and data analysis was done with NanoScope (Bruker, USA) and the open-source Gwyddion package.^[35] For liquid-cell AFM imaging, DNA origami was incubated on mica for 1 min, buffer-washed to remove the unbound plates, while the structure was kept in liquid for imaging without any further drying. The washing and imaging buffer was supplemented with an additional 1×10^{-3} M NiCl_2 for

better attachment of the origami to mica, which resulted in more stable AFM imaging.

Supporting Information

Supporting Information is available from the Wiley Online Library or from the author.

Acknowledgements

This work was supported by the Netherlands organization for scientific research (NWO/OCW), as part of the Frontiers of Nanoscience program. Funding from the ERC advanced grants, NEMinTEM 267922 and SynDiv 669598, is also appreciated. The authors acknowledge the FEI NanoPort in Eindhoven for access to the Helios dual beam microscope, especially the kind efforts of Nico Clemens. J.-Y.H. and J.K. acknowledge support from the US AFOSR FATE MURI, Grant No. FA9550-15-1-0514. A.N.A. acknowledges funding from the NanoNextNL (program 07A.05) and thanks Philip Ketterer (TU Munich) for valuable discussions.

Conflict of Interest

The authors declare no conflict of interest.

- [1] R. M. Westervelt, *Science* **2008**, *320*, 324.
- [2] Y. Liu, X. Dong, P. Chen, *Chem. Soc. Rev.* **2012**, *41*, 2283.
- [3] J. Jeon, M. S. Lodge, B. D. Dawson, M. Ishigami, F. Shewmaker, B. Chen, *Biochim. Biophys. Acta* **2013**, *1830*, 3807.
- [4] R. S. Pantelic, J. W. Suk, C. W. Magnuson, J. C. Meyer, P. Wachsmuth, U. Kaiser, R. S. Ruoff, H. Stahlberg, *J. Struct. Biol.* **2011**, *174*, 234.
- [5] R. Zan, Q. M. Ramasse, R. Jalil, T. Georgiou, U. Bangert, K. S. Novoselov, *ACS Nano* **2013**, *7*, 10167.
- [6] C. Wang, Q. Qiao, T. Shokuhfar, R. F. Klie, *Adv. Mater.* **2014**, *26*, 3410.
- [7] M. R. Jones, N. C. Seeman, C. A. Mirkin, *Science* **2015**, *347*, 1260901.
- [8] S. Woo, P. W. K. Rothemund, *Nat. Chem.* **2011**, *3*, 620.
- [9] P. W. K. Rothemund, *Nature* **2006**, *440*, 297.
- [10] S. M. Douglas, A. H. Marblestone, S. Teerapittayanon, A. Vazquez, G. M. Church, W. M. Shih, *Nucleic Acids Res.* **2009**, *37*, 5001.
- [11] J. D. Griffith, S. Lee, Y. H. Wang, *Curr. Opin. Struct. Biol.* **1997**, *7*, 362.
- [12] M. Marini, A. Falqui, M. Moretti, T. Limongi, M. Allione, A. Genovese, S. Lopatin, L. Tirinato, G. Das, B. Torre, A. Giugni, F. Gentile, P. Candeloro, E. Di Fabrizio, *Sci. Adv.* **2015**, *1*, 1.
- [13] M. Marini, T. Limongi, A. Falqui, A. Genovese, M. Allione, M. Moretti, S. Lopatin, L. Tirinato, G. Das, B. Torre, A. Giugni, F. Cesca, F. Benfenati, E. Di Fabrizio, *Nanoscale* **2017**, *9*, 2768.
- [14] F. Gentile, M. Moretti, T. Limongi, A. Falqui, G. Bertoni, A. Scarpellini, S. Santoriello, L. Maragliano, R. Proietti Zaccaria, E. Di Fabrizio, *Nano Lett.* **2012**, *12*, 6453.
- [15] S. Buckhout-White, J. T. Robinson, N. D. Bassim, E. R. Goldman, I. L. Medintz, M. G. Ancona, *Soft Matter* **2013**, *9*, 1414.
- [16] K. Nagayama, R. Danev, *Philos. Trans. R. Soc., B* **2008**, *363*, 2153.

- [17] B. J. Pages, D. L. Ang, E. P. Wright, J. R. Aldrich-Wright, *Dalton Trans.* **2015**, 44, 3505.
- [18] R. Erni, *Aberration-Corrected Imaging in Transmission Electron Microscopy*, Imperial College Press, London, UK **2010**.
- [19] R. F. Egerton, F. Wang, P. A. Crozier, *Microsc. Microanal.* **2006**, 12, 65.
- [20] P. A. Midgley, M. Weyland, J. M. Thomas, B. F. G. Johnson, *Chem. Commun.* **2001**, 907.
- [21] R. M. Glaeser, *J. Ultrastruct. Res.* **1971**, 36, 466.
- [22] C. Zhang, Q. Xu, P. J. Peters, H. Zandbergen, *Ultramicroscopy* **2013**, 134, 200.
- [23] R. F. Egerton, P. Li, M. Malac, *Micron* **2004**, 35, 399.
- [24] G. Algara-Siller, S. Kurasch, M. Sedighi, O. Lehtinen, U. Kaiser, *Appl. Phys. Lett.* **2013**, 103, 203107.
- [25] R. M. Glaeser, *Nat. Methods* **2016**, 13, 28.
- [26] G. Algara-Siller, O. Lehtinen, A. Turchanin, U. Kaiser, *Appl. Phys. Lett.* **2014**, 104, 153115.
- [27] B. S. Husale, S. Sahoo, A. Radenovic, F. Traversi, P. Annibale, A. Kis, *Langmuir* **2010**, 26, 18078.
- [28] N. S. Green, M. L. Norton, *Anal. Chim. Acta* **2015**, 853, 127.
- [29] W. Liu, H. Zhong, R. Wang, N. C. Seeman, *Angew. Chem. Int. Ed.* **2011**, 50, 264.
- [30] R. Campos, S. Zhang, J. M. Majikes, L. C. C. Ferraz, T. H. LaBean, M. D. Dong, E. E. Ferapontova, *Chem. Commun.* **2015**, 51, 14111.
- [31] J. M. Yun, K. N. Kim, J. Y. Kim, D. O. Shin, W. J. Lee, S. H. Lee, M. Lieberman, S. O. Kim, *Angew. Chem. Int. Ed.* **2012**, 51, 912.
- [32] R. S. Pantelic, W. Fu, C. Schoenenberger, H. Stahlberg, *Appl. Phys. Lett.* **2014**, 104, 134103.
- [33] C. E. Castro, F. Kilchherr, D.-N. Kim, E. L. Shiao, T. Wauer, P. Wortmann, M. Bathe, H. Dietz, *Nat. Methods* **2011**, 8, 221.
- [34] W. Regan, N. Alem, B. Alemán, B. Geng, Ç. Girit, L. Maserati, F. Wang, M. Crommie, A. Zettl, *Appl. Phys. Lett.* **2010**, 96, 113102.
- [35] D. Nečas, P. Klapetek, *Cent. Eur. J. Phys.* **2012**, 10, 181.

Received: March 17, 2017

Revised: April 29, 2017

Published online: